Electronic Supplementary Material (ESI) for Dalton Transactions
This journal is © The Royal Society of Chemistry 2013

Supplementary information for Crystal structures and variable magnetism of $PbCu_2(XO_3)_2Cl_2$ with X = Se, Te

Peter S. Berdonosov, Oleg Janson, Andrey V. Olenev,
Sergey V. Krivovichev, Helge Rosner, Valery A. Dolgikh, and Alexander A. Tsirlin

TABLE S1. Crystal data and structure refinement for $PbCu_2(SeO_3)_2Cl_2$ and $PbCu_2(TeO_3)_2Cl_2$.

Empirical formula	$PbCu_2(SeO_3)_2Cl_2$	$PbCu_2(TeO_3)_2Cl_2$
Crystal system	monoclinic	monoclinic
Space group	$C2/c$ (No. 15)	$P12_11$ (No. 4)
a (Å)	13.0560(10)	7.2401(2)
b (Å)	9.5567(9)	7.2688(2)
c (Å)	6.9006(6)	8.2846(2)
β (deg)	90.529(7)	96.416(2)
Volume (Å^3)	860.97(13)	433.26(2)
Z	4	2
Calculated density (g/cm^3)	5.085	5.798
Absorption coefficient (mm^{-1})	33.465	31.450
Instrument	STOE IPDS	STOE StadiVari
Crystal size (mm)	$0.1 \times 0.05 \times 0.02$	$0.2 \times 0.12 \times 0.08$
θ range (deg)	$2.64 - 29.13$	$2.83 - 25.99$
h, k, l ranges	$-17 \le h \le 17$	$-5 \le h \le 8$
	$-13 \le k \le 11$	$-8 \le k \le 7$
	$-9 \le l \le 9$	$10 \le l \le 9$
No. of reflections	2954	1840
Independent reflections	1157 ($R_{\rm int} = 0.067$)	3277 ($R_{\rm int} = 0.0809$)
Refinement method	full-matrix least-squares on F^2, Shelx	
Data/restraints/parameters	1157/0/63	1412/1/119
Goodness-of-fit on F^2	1.057	1.031
$R(I > 2\sigma(I))$	$R_1 = 0.0298, wR_2 = 0.0537$	$R_1 = 0.0540, wR_2 = 0.1396$
R (all data)	$R_1 = 0.0371, wR_2 = 0.0553$	$R_1 = 0.0570, wR_2 = 0.1408$
Extinction coefficient	0.00274(16)	0.040(4)
Largest diff. peak and hole (e/Å^3)	1.618, −1.289	4.42, −3.44

TABLE S2. Atomic positions and isotropic atomic displacement parameters $U_{\rm iso}$ (in 10^{-2} Å^2) in $PbCu_2(SeO_3)_2Cl_2$. $U_{\rm iso}$ are defined as one third of the trace of the orthogonalized U_{ij} tensor.

	Position	x/a	y/b	z/c	$U_{\rm iso}$
Pb	4e	0.5	0.15837(4)	0.25	1.3(1)
Se	8f	0.66777(4)	0.39768(7)	0.08750(8)	1.0(1)
Cu(1)	4e	0.5	0.38774(13)	0.75	1.4(1)
Cu(2)	4c	0.75	0.75	0	1.5(1)
Cl	8f	0.62544(12)	0.8968(2)	0.1207(3)	2.2(1)
O(1)	8f	0.5477(3)	0.3466(5)	0.0081(6)	1.5(1)
O(2)	8f	0.3394(3)	0.2877(5)	0.2159(7)	1.7(1)
O(3)	8f	0.6431(3)	0.5576(5)	0.1759(7)	1.6(1)

TABLE S3. Atomic positions and isotropic atomic displacement parameters $U_{\rm iso}$ (in 10^{-2} Å^2) in $PbCu_2(TeO_3)_2Cl_2$. $U_{\rm iso}$ are defined as one third of the trace of the orthogonalized U_{ij} tensor. All atoms are in the general position $2a$ of the $P2_1$ space group.

	x/a	y/b	z/c	$U_{\rm iso}$
Pb	0.12805(14)	0.1000(2)	0.06175(14)	1.35(5)
Te(1)	0.8728(2)	0.9580(3)	0.6128(2)	0.65(6)
Te(2)	0.3551(2)	0.7298(3)	0.7679(2)	0.64(6)
Cu(1)	0.3622(4)	0.5923(7)	0.0902(4)	0.85(8)
Cu(2)	0.3180(5)	0.1085(7)	0.5868(5)	1.01(8)
Cl(1)	0.5533(11)	0.3254(12)	0.6245(10)	1.6(2)
Cl(2)	0.1106(12)	0.3397(12)	0.7709(11)	1.7(2)
O(1)	0.459(3)	0.969(3)	0.760(2)	0.8(4)
O(2)	0.853(3)	0.975(4)	0.835(3)	1.3(5)
O(3)	0.128(3)	0.918(3)	0.624(3)	1.1(5)
O(4)	0.204(3)	0.755(3)	0.941(3)	0.9(4)
O(5)	0.809(3)	0.710(4)	0.607(3)	1.3(5)
O(6)	0.540(3)	0.650(3)	0.936(3)	1.0(5)

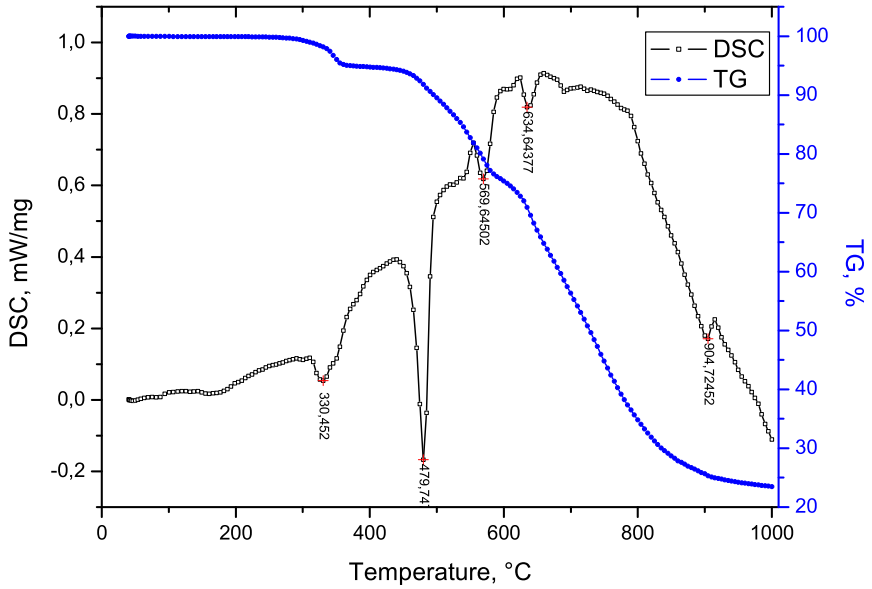

FIG. S1. Thermal decomposition of $PbCu_2(SeO_3)_2Cl_2$ studied by differential scanning calorimetry (DSC) and thermogravimetry (TG). The multi-step decomposition process starts at $\sim$300°C. The heating rate is 10 °C/min.

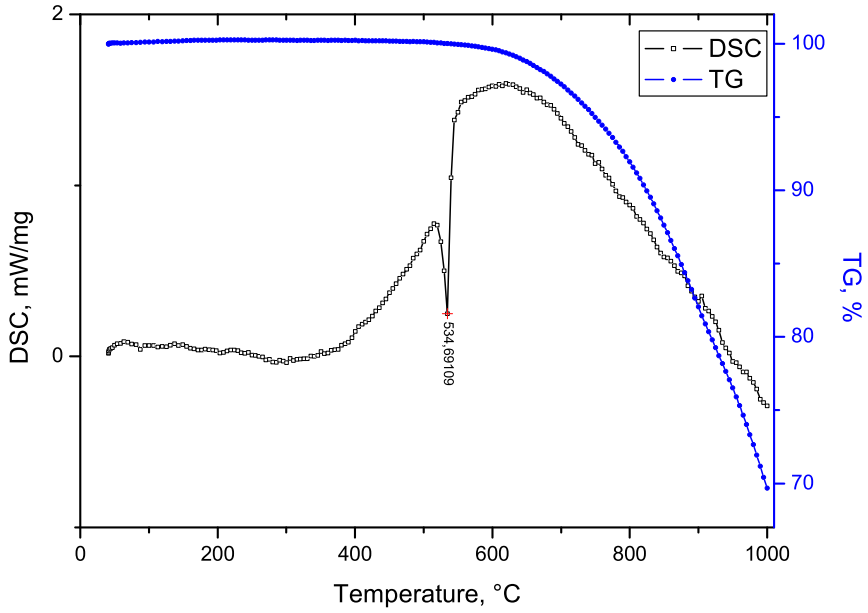

FIG. S2. Thermal decomposition of $PbCu_2(TeO_3)_2Cl_2$ studied by differential scanning calorimetry (DSC) and thermogravimetry (TG). Thermal decomposition starts starts at ~ 500°C, but it remains incomplete even at 1000°C. The heating rate is 10 °C/min.

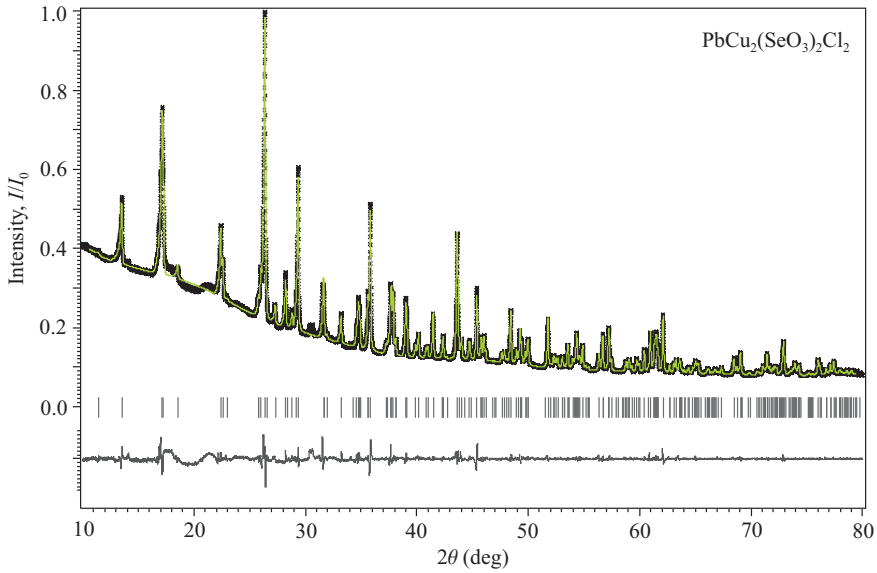

FIG. S3. Powder pattern of $PbCu_2(SeO_3)_2Cl_2$ (crystals selected from the batch and used for the magnetic susceptibility measurements) and its fit using the structural data obtained from the single crystal. The high background at low angles is due to a very small amount of sample (5 mg). Broad features at $2\theta = 18°$ and 22° are from vaseline that was used as adhesive. A weak reflection at $2\theta = 31.5°$ belongs to the residual foreign phase (ferromagnetic impurity).

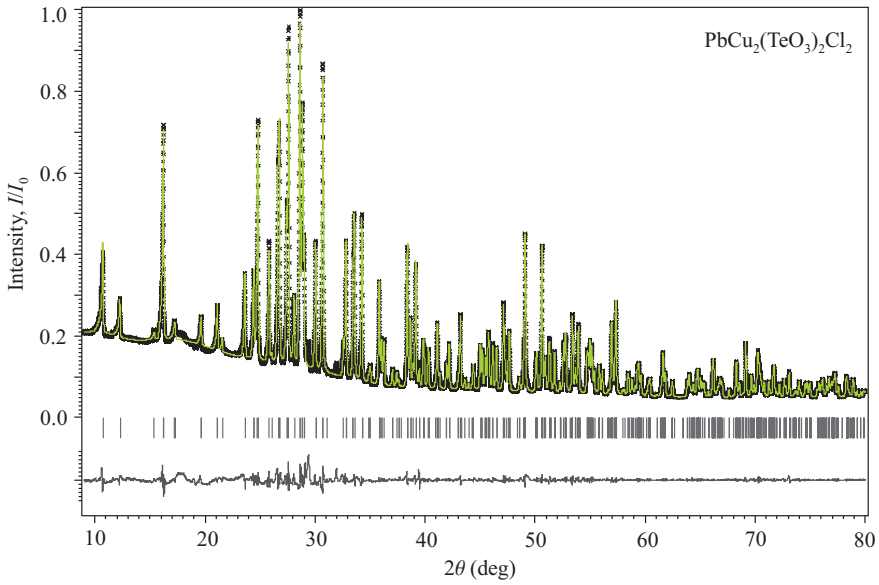

FIG. S4. Powder pattern of $PbCu_2(SeO_3)_2Cl_2$ and its fit using the structural data obtained from the single crystal. The broad feature at $2\theta = 18^\circ$ is from vaseline that was used as adhesive. Reflections of impurities ($CuTe_2O_5$, $3PbTeO_3 \times 2H_2O$) are barely visible on this scale.

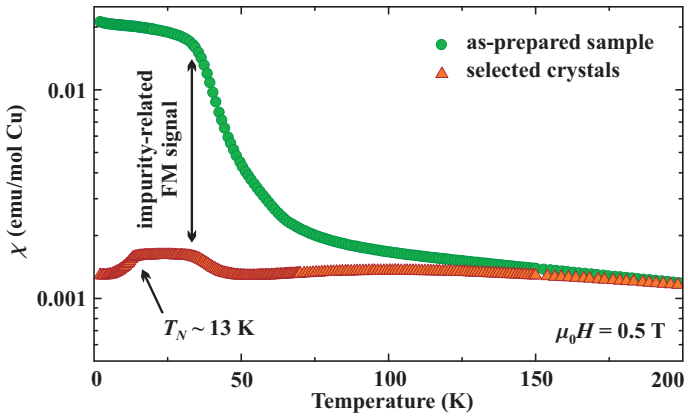

FIG. S5. Magnetic susceptibility of the as-prepared sample of $PbCu_2(SeO_3)_2Cl_2$ (circles) and selected batch of crystals (triangles).

TABLE S4. The leading magnetic exchange couplings in $PbCu_2(SeO_3)_2Cl_2$ and $PbCu_2(TeO_3)_2Cl_2$: Cu–Cu distances ($d_{\text{Cu–Cu}}$, in Å), transfer integrals t_{ij} (in meV), antiferromagnetic (J_{ij}^{AFM}) and ferromagnetic (J_{ij}^{FM}) contributions to the total magnetic exchange (J_{ij}, in K). The t_{ij} terms are evaluated from the GGA bands using Wannier functions. J_{ij}^{AFM} are approximated using $J_{ij}^{\text{AFM}} = 4t_{ij}^2/U_{\text{eff}}$ adopting $U_{\text{eff}} = 4.5$ eV. The ferromagnetic contribution J^{FM} is evaluated as the difference between J_{ij}^{AFM} and J_{ij}, where the latter term is estimated from the GGA+U calculations.

	$PbCu_2(SeO_3)_2Cl_2$				
	$d_{\text{Cu–Cu}}$	t_{ij}	J^{AFM}	J^{FM}	J_{ij}
J_1	6.23	−143	211	−45	166
J_{ic1}	8.65	−47	23	−6	17
J_{ic2}	8.09	−70	51	−11	39
	$PbCu_2(TeO_3)_2Cl_2$				
	$d_{\text{Cu–Cu}}$	t_{ij}	J^{AFM}	J^{FM}	J_{ij}
J	3.34	143	211	−15	196
J'	5.59	−90	84	–	86

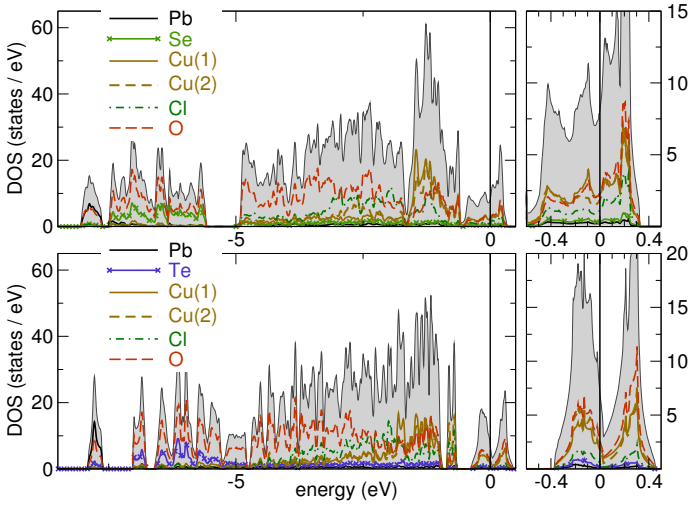

FIG. S6. GGA total (shaded) and partial (lines) DOS for $PbCu_2(SeO_3)_2Cl_2$ (top) and $PbCu_2(TeO_3)_2Cl_2$ (bottom). The magnetically active states around the Fermi level are zoomed in the right panels. Number of states is given per primitive cell. Fermi level is at zero energy.

Electronic Supplementary Material (ESI) for Dalton Transactions
This journal is © The Royal Society of Chemistry 2013

DETAILS OF DFT CALCULATIONS

The $3d^9$ electronic configuration of Cu^{2+} should lead to a partial filling of the $3d$ bands and, therefore, to the metallic behavior. However, strong electronic correlations that are inherent to the strongly localized Cu $3d$ states trigger the formation of a band gap and the overall insulating behavior.

Electronic correlations are many-body effects that can not be accounted for on the standard DFT level. This explains the metallic ground state indicated by nonzero density of states at the Fermi level, in both LDA and GGA calculations (both functionals yield nearly indistinguishable density of states [DOS] and band dispersions), see Fig. S6. The correct insulating state can be reproduced by supplying the standard DFT functionals with the strong Coulomb correlations in the Cu $3d$ shell. This is done in two complementary approaches: i) on the model level, or ii) by a static mean-field treatment within the DFT+U formalism.

In standard GGA, both $PbCu_2(SeO_3)_2Cl_2$ and $PbCu_2(TeO_3)_2Cl_2$ feature a well-structured valence band (Fig. S6): the bottom edge shows a peak of Pb–O states (around -8 eV), the energy range between -7.5 eV and -5.5 eV is dominated by Se/Te and O states, while the rest of the valence band is formed predominantly by Cu, O, and Cl states. The magnetically active states are located in a close vicinity of the Fermi level. In $PbCu_2(TeO_3)_2Cl_2$, these states are well-separated from the rest of the valence band. In $PbCu_2(SeO_3)_2Cl_2$, these states are separated from the rest of the valence band by a dip in the DOS spectrum.

In cuprates, the magnetically relevant states are conveniently described in terms of atomic-like orbitals. In the most common case of a CuO_4 plaquette, it is a single molecular-like orbital comprising the Cu $3d$ orbital stretched towards the four O atoms, and the four σ-bonded O $2p$ orbitals. These states can be denoted according to the local coordinate system, with the x and y axes running along the Cu–O bond, and the z axis perpendicular to the plaquette plane. In this setup, the magnetically active orbital of Cu has the $x^2 - y^2$ character. This is the case for Cu(1) in both $PbCu_2(SeO_3)_2Cl_2$ and $PbCu_2(TeO_3)_2Cl_2$.

In the case of Cu(2), the same arguments apply. We find the magnetic $d_{x^2-y^2}$ orbital, with the x and y axes running along the four shortest Cu–O/Cl bonds that are nearly coplanar. The two long Cu–O (X = Se) or Cu–Cl (X = Te) bonds are directed along the local z axis. The respective atoms do not contribute to the magnetic orbital and do not facilitate the magnetic interaction. This way, we identify the $Cu(2)O_3Cl$ and $Cu(2)O_2Cl_2$ plaquettes in $PbCu_2(SeO_3)_2Cl_2$ and $PbCu_2(TeO_3)_2Cl_2$, respectively.

The dp_σ molecular-like orbitals form a convenient basis set for an effective one-orbital model that describes electron transfer between different Cu^{2+} sites. The energy terms t_{ij} responsible for the electron transfer should be supplemented by a Coulomb interaction term that penalizes the doubly occupied states. For sufficiently strong correlations, the AFM exchange J_{ij}^{AFM} is proportional to t_{ij}^2, where t_{ij} is related to the probability of the electron hopping between sites i and j. The t_{ij} terms can be evaluated directly from LDA or GGA band structure calculations using localized Wannier functions (numerical values for the relevant terms are given in Table S4).